



A solution for the frictional resistance in macro-block limit analysis of non-periodic masonry

Marco Francesco Funari^{a,b,*}, Bora Pulatsu^c, Simon Szabó^b, Paulo B. Lourenço^b

^a Department of Civil and Environmental Engineering, University of Surrey, Guildford GU2 7XH, UK

^b Department of Civil Engineering, University of Minho, ISE, Guimarães 4800 - 058, Portugal

^c Department of Civil and Environmental Engineering, Carleton University, Ottawa K1S 5B6, Canada

ARTICLE INFO

Keywords:

Limit analysis
Non-periodic masonry
Frictional resistance
Macro-block approach
Easy-to-use digital tools
Discrete Element Method

ABSTRACT

This paper proposes a general equation to assess the crack inclination upper threshold when non-periodic textures characterise masonry walls. The proposed formulation introduces the computation of the frictional resistance at the macro-block interface by evaluating two masonry quality indexes, i.e., vertical and horizontal lines of trace. The proposed equation is adopted in conjunction with a macro-block limit analysis formulation in which the failure mechanism is parametrised and formulated according to the upper bound limit analysis theorem, coupled with a heuristic solver that is able to minimise the load multiplier and identify the geometry of the associated macro-block. The proposed analytical model is verified in a number of case studies by comparing advanced DEM simulations and numerical results arising from the literature.

1. Introduction

Given its important role for economies and societies, the assessment, preventive conservation and maintenance of historical masonry structures continue to stand as major priorities of the overall political strategy at the European level. In this context, the earthquake protection of historical masonry structures assumes particular relevance because of their non-negligible seismic vulnerability. The tangible and intangible value of this type of ancient buildings is further enhanced by the artworks located therein, such as sculptures, paintings and frescos, among others. This means that when a disaster involves historical centres, it is likely that buildings, as well as artworks, are damaged, producing: i) a physical loss of artistic and historical materials; ii) an immaterial loss of memory and cultural identity for the people to whom that legacy “belongs”; and iii) difficulties in the action of the Civil Protection in assisting the population affected by the disaster [1–3].

In this regard, to preserve historical masonry structures, several researchers focused on implementing advanced computational modelling strategies. The overall classification of these tools is mainly made between numerical and analytical approaches [4–7].

Numerical approaches are typically implemented in the Finite Element Method (FEM) [8–14] or Discrete Element Method (DEM) [15–21] framework. Such approaches model the masonry material using

different representation scales, i.e., equivalent continuum, macro-blocks, or discrete representations. FEM allows more versatile application as masonry can be represented either through a homogeneous equivalent media (designated macro-modelling) or by a discrete representation of units and joints (designated as simplified micro-modelling) [10,22]. DEM is well suited for masonries (both dry- and mortared joints [23–25]), and focuses on non-homogeneous material representations. The computational procedure of DEM provides a great advantage to consider the complex geometrical features of masonry in the structural analysis [25–27]. Typically, in a DEM-based discontinuum analysis, masonry constructions are represented via a system of distinct polyhedral blocks that can interact based on the point contact hypothesis [28,29]. The mechanical interaction among adjacent blocks is formulated through the prescribed contact stress-displacement laws with different linear or nonlinear behaviour. Rigid and/or deformable blocks may be used depending on the research question and the expected outcomes from the numerical model, also considering a compromise between computational cost and accuracy. As shown by various studies in the literature, DEM offers a wide range of solutions to simulate regular and irregular, discontinuous medium subjected to quasi-static, dynamic, or coupled thermo-mechanical loadings from mesoscale to macro-scale [26,30–33].

Nonetheless, in addition to the significant amount of data needed to

* Corresponding author at: Department of Civil and Environmental Engineering, University of Surrey, Guildford GU2 7XH, UK.
E-mail address: m.funari@surrey.ac.uk (M.F. Funari).

<https://doi.org/10.1016/j.istruc.2022.06.072>

Received 22 April 2022; Received in revised form 27 June 2022; Accepted 28 June 2022

Available online 13 July 2022

2352-0124/© 2022 Institution of Structural Engineers. Published by Elsevier Ltd. All rights reserved.

characterise the nonlinear response of materials, the analysis can be time-consuming and computationally expensive, particularly when the objective is to estimate the ductility level of the structure (as required in design codes for performance based seismic assessment). Furthermore, despite their reliability, the computational efficiency of the available numerical methods is rarely compatible with the need to have a rigorous real-time post- or pre-earthquake assessment [34]. Hence, several research groups have been developing alternative modelling approaches and practical tools to decrease the computational cost of nonlinear static and dynamic analyses [35–38].

When a disaster happens, the structural safety assessment of a huge number of constructions, including building aggregates, churches and other monuments, must be performed in a short time. In addition, most professionals lack the necessary knowledge to use adequately advanced simulation tools. Finally, the requirements of using these advanced tools are, often, not in line with the available time and budget. Therefore, despite the extraordinary computational power available thanks to state of the art CPU processors and advanced software, often structural engineers adopt analytical approaches based on limit analysis (LA) theorems. These have the great advantage of requiring only a few material properties but, inevitably, rely on a very simplified material model [39–43]. In literature, LA has been formulated at both macro and micro scales. Micro LA formulations account for a unit by unit description with an introduction of interfaces that represent masonry joints. In Livesley [44], a formal procedure for finding the limit load of any structure formed from rigid blocks is given. In this formulation, the limit of the shear force at a block interface was computed according to Coulomb's friction theory. In Ferris and Tin-Loi [45], the computation of the load multiplier of discrete rigid block systems, characterised by frictional (non-associative) and tensionless contact interfaces, was formulated and solved through a Mathematical Program with Equilibrium Constraints (MPEC). Similarly, in Gilbert et al. [46], a simple iterative procedure which involves the successive solution of linear programming sub-problems is adopted. Recently, several research groups proposed customised computer program interfaces, which can also account for 3D rigid block assemblages [47,48].

One can note that micro LA requires unit by unit representation, which is still a challenging task, particularly when non-periodic or rubble masonry patterns affect the behaviour of structures under investigation. For this reason, macro LA is considered as a practical and useful tool for the rapid and engineering assessment of the collapse load of masonry structures [49], and national and international standards suggest its use [50]. In this framework, following post-earthquake damage surveys carried out after the Irpinia and Syracuse earthquakes in Italy, an abacus of local failure mechanisms was compiled [51]. Thus, algorithms able to find the most reasonable collapse mechanisms into user-defined analysis routines have been implemented [52–56]. In Fortunato et al. [57], a numerical procedure for the LA of 2D masonry structures subject to arbitrary loading was developed. Similarly, in the framework of LA methods, other authors have proposed *meta*-heuristic approaches (i.e., Genetic Algorithms) as a tool to explore the value of loads associated with considered collapse mechanisms [58]. In Casapulla et al. [53], a simplified procedure for the prediction of the collapse load and the failure mechanism of in-plane loaded masonry walls was proposed by taking into consideration frictional resistance. Recently another study upgraded this procedure in order to account for the actual frictional resistance [59]. However, the adopted formulation accounts only for regular masonry patterns.

Indeed, the literature survey underlines the lack of macro LA formulation accounting for non-periodic or rubble masonry patterns. This is mainly due to the difficulties in evaluating the actual frictional resistance generated when irregular patterns affect masonry walls. The most rational solution to cover this gap is to refer to studies developing geometric masonry quality indexes to assess the quality of the masonry arrangements [60]. Some of these studies found useful correlations with the mechanical parameters [61], such as compressive strength, shear

strength and elastic modulus. However, no studies correlate such quality indexes with the actual capacity of the irregular masonry pattern to produce in-plane frictional resistance.

In order to address this knowledge gap, the present study aims to implement and validate a new theory for the computation of the frictional resistance involved in the in-plane sliding-rocking mechanism suitable for non-periodic and rubble masonry textures. The proposed theory is integrated within the framework of the upper-bound theorem of LA [55,59], with the methodology detailed next:

Develop a general equation to assess the crack inclination upper threshold that characterises masonry patterns when the structures are affected by the in-plane sliding-rocking failure mechanisms.
Implement the macro-block LA formulation within a Rhino 3D + Grasshopper [62,63] plugin. As an output, the tool provides the horizontal load multiplier and the geometry of the failure mechanism.

The results obtained by the macro-block LA are validated against a detailed DEM model. Horizontal load multipliers are compared with the expected failure mechanism for several wall configurations.

The novelties of the study are twofold: i) identification of a frictional resistance law that accounts for non-periodic masonry patterns; and ii) definition of a general procedure that guides practitioners from the inspection to the assessment of the seismic capacity of masonry buildings by using macro-block LA.

The paper is divided as follows. Section 2 presents the macro-block LA formulation for in-plane sliding rocking mechanism. In Section 3 the proposed formulation to compute crack inclination upper threshold is analytically developed. Section 4 integrates the proposed formula within a macro-block upper bound LA formulation. Section 5 describes the DEM adopted as a reference for the validation of the LA tool. Section 6 is devoted to validate the formulation through real and artificial case studies. Finally, relevant conclusions are drawn in Section 7.

2. Overview of existing macro-block formulation for the in-plane sliding-rocking failure mechanism

The in-plane sliding-rocking failure mechanism of unreinforced masonry structures, through macro-block LA, has been extensively investigated in the literature [53,55,59,64].

Fig. 1 shows an assemblage of dry rigid units with the same dimensions and arranged with a regular bond type. Regarding the portion of masonry involved in the mechanism, the macro-block model is based on the assumption that the failure is defined by a crack line with an inclination equal to α_c , which separates the structure into macro-blocks. Once the sliding-rocking mechanism is pre-defined, the equation of equilibrium can be formulated by means of the virtual work principle in which the only unknown is the horizontal load multiplier. The external virtual work contains both the overturning as well as the stabilising works performed by the inertial forces, whereas the internal work is derived from the friction force at contact interfaces (Fig. 1):

$$\begin{aligned} \delta W_{ext} &= \lambda \cdot W_{OBC} \cdot \delta_{O,OBC} - W_{OBC} \cdot \delta_{S,OBC} \\ \delta W_{int} &= F_{real} \cdot \delta_{Sf} \end{aligned} \quad (1)$$

where W_{OBC} is the inertial force arising from the self-weight of the macro-block OBC, $\delta_{O,OBC}$ and $\delta_{S,OBC}$ are the virtual overturning and stabilising displacements of the centre of gravity of the macro-block, and F_{real} is the frictional resistance generated by the wall. The formulation reported in Eq. (1) may be easily generalised to account for possible overload and a transverse façade that collapses out-of-plane; in this case, the reader can refer to [35,59].

Regarding the internal work, it is worth remarking that the evaluation of the frictional resistance is not an easy task for masonry constituted by a regular or a non-periodic masonry pattern since it is difficult

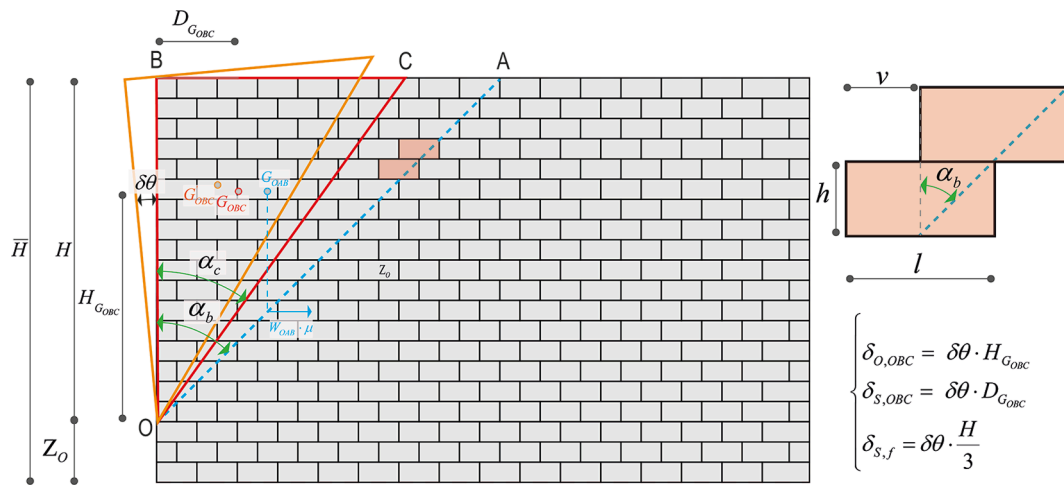


Fig. 1. Kinematic description of the sliding-rocking mechanism for an in-plane shear wall.

to estimate the number of active sliding interfaces along the generic crack. When pure sliding occurs, the frictional resistance may be easily computed accordingly to Coulomb’s law as the product weight of the triangle OAB by the frictional coefficient μ [59], where the OAB is the macroblock identified by the maximum admissible crack line orientation. However, failure mechanisms often involve mix-mode sliding-rocking with consequently uplifting of the blocks that reduce the number of the bed joints in full contact. In order to take into consideration this phenomenon and to compute the actual frictional resistance, a proposal was made in Casapulla et al. [59] to compute the actual value of the frictional resistance for the moving part of the wall as a weighted value as a function of the inclinations of the crack line. This is given by:

$$F_{real} = W_{OAB} \cdot \mu \cdot \left(1 - \frac{\alpha_c}{\alpha_b}\right) \quad (2)$$

with:

$$W_{OAB} = \frac{(\bar{H} - Z_0)^2}{2} \cdot \tan(\alpha_b) \cdot t_w \cdot \gamma \quad (3)$$

where t_w is the thickness of the in-plane wall, and γ is the specific weight of the masonry, α_c is the actual crack inclination and α_b is the crack inclination upper threshold (which depends on the geometry of the block, see Fig. 1):

$$\tan(\alpha_b) = \frac{v}{h} \quad (4)$$

Here, v and h are half-width and height of the unit blocks, respectively.

Hence, the horizontal load multiplier can be evaluated by equating external and internal virtual work and solving for λ . According to the upper-bound theorem of the LA, the computation of the horizontal load multiplier requires the solution of a constrained minimisation problem in which the parameters defining the failure mechanism’s geometry, i.e., α_c and Z_0 , are adopted as variables to explore all the panorama of possible solutions:

$$\begin{aligned} &\text{minimise : } \lambda \\ &\text{subject to: } Z_0 \leq \bar{H} \\ &0 \leq \alpha_c \leq \alpha_b \end{aligned} \quad (5)$$

where Z_0 is the height position of the pivot point and \bar{H} is the total height of the wall.

One should note that the parameter Z_0 only plays a role in case of overload or the presence of a transverse façade [55].

3. Frictional resistance definition for different masonry typologies

It is worth noting how, despite the good accuracy of both horizontal multiplier and geometry of the failure mechanisms, the analytical formulation defined in Eqs. (1)–(5) may only be adopted for regular assemblages of same size units, strongly limiting the field of applications of the macro-block LA.

In order to make the aforementioned analytical formulation suitable for masonry walls composed of non-periodic patterns, the contribution arising from the definition of the frictional resistance must be reformulated. The challenge is to avoid Eq. (4) dependency on the block aspect ratio and propose a procedure based on the inspection of a representative masonry pattern window (RMPW) to define specific masonry quality indexes that serve as engineering parameters to define the crack inclination upper threshold α_b for different masonries, i.e., from regular to rubble.

Remark 1. It is well known that to characterise/classify masonry patterns, one can focus on the definition of RMPW and compute masonry quality indexes and find their correlation with specific properties of the masonry macro behaviour [60,61].

3.1. Regular and non-regular coursed squared masonries

Fig. 2 represents two in-plane shear walls constituted by regular or non-regular coursed squared masonries, subjected to horizontal inertial forces generating the sliding-rocking mechanism. The blue traced lines represent the identification of the crack inclination upper thresholds. In order to compute α_b , one has to compute the sums of the horizontal and vertical lines defined by the blue polyline, respectively and perform their ratio:

$$\tan(\alpha_b) = \frac{\sum_{i=1}^{n_c} v_i}{\sum_{i=1}^{n_c} h_i} \quad (6)$$

n_c is the number of courses, v_i and h_i are the horizontal interfaces’ length and height of the unit blocks traced at the specific course, respectively.

Eq. (6) is valid for both regular (Fig. 2a) and non-regular coursed squared masonries (Fig. 2b), with the only difference that in the case of regular masonry, the evaluation of α_b only depends by the knowledge of the unit aspect ratio, since all the units have equal v and h (see Eq. (4)).

Inspired by Remark 1, instead of computing the crack inclination upper thresholds referring to the entire wall, it is here proposed to refer to an RMPW and calculate α_b accordingly:

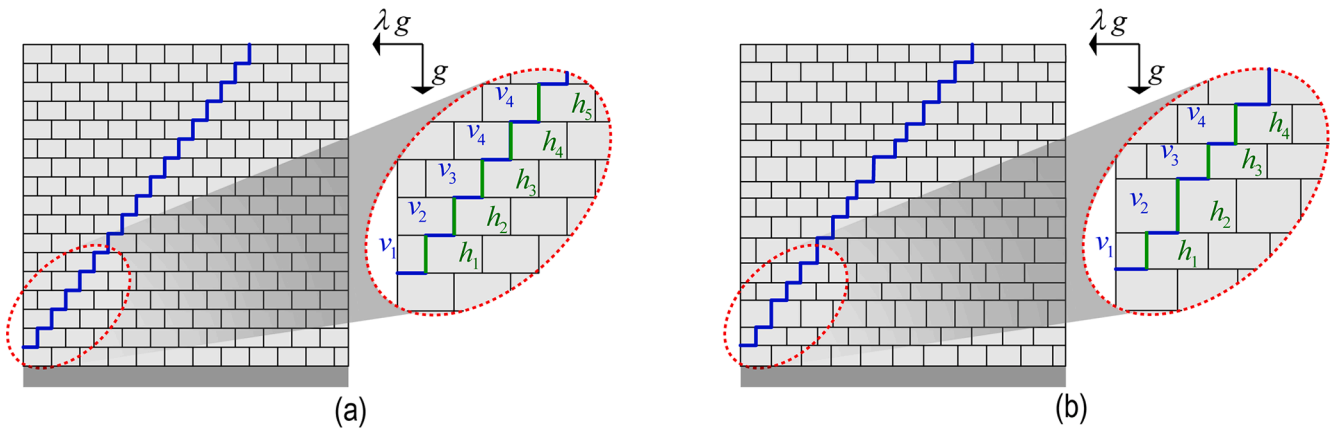


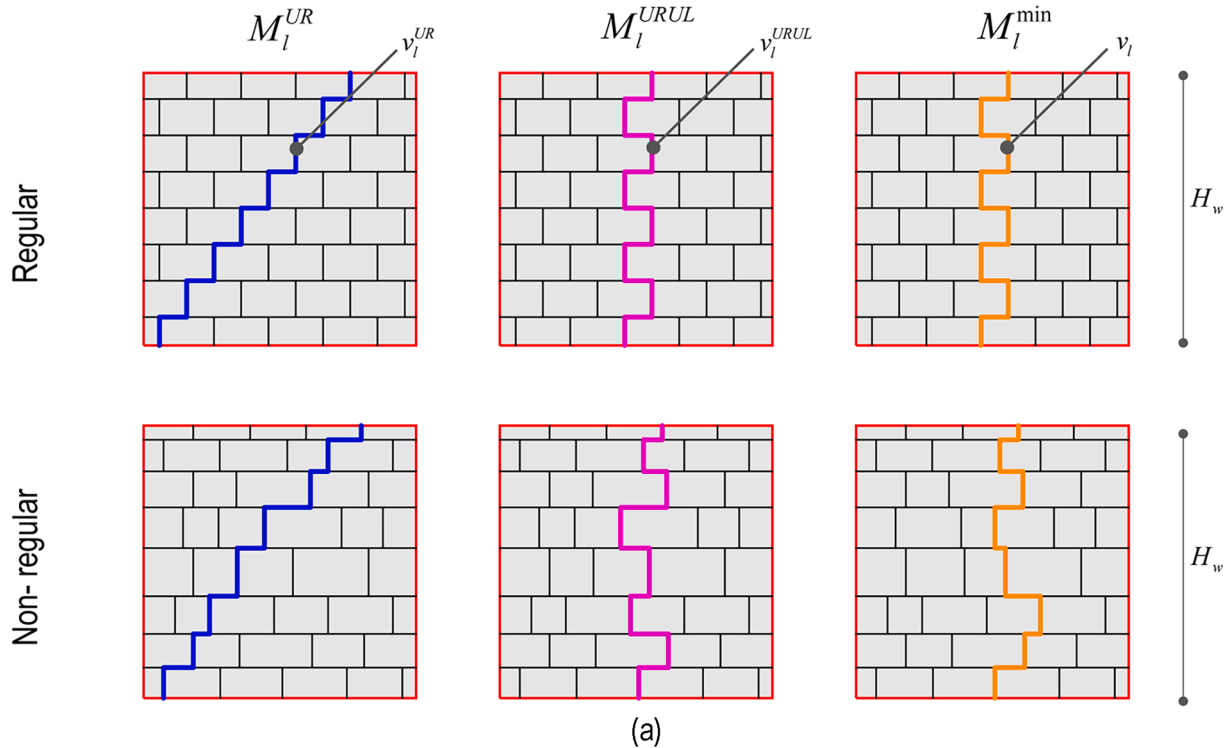
Fig. 2. In-plane shear wall: (a) Regular Pattern; (b) Non-Regular Pattern.

$$\tan(\alpha_b) = \frac{\sum_{i=1}^{n_c} v_i}{\sum_{i=1}^{n_c+1} h_i} \quad (7)$$

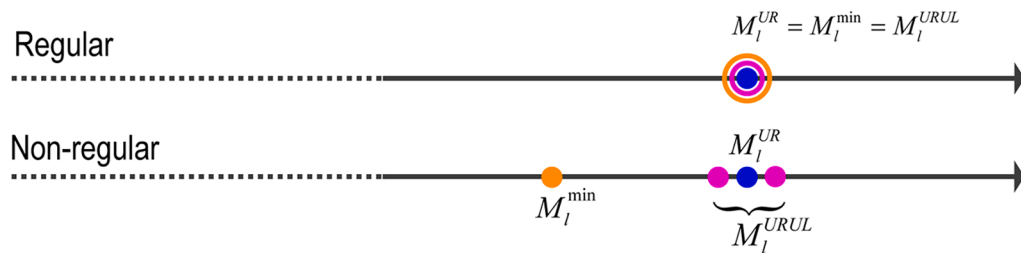
It is worth remarking that, in this case, n_c refers to the number of courses inside the RMPW.

At this stage, the blue traced line inside the RMPW (see Fig. 3a first column), can be adopted in order to define a masonry quality index.

Such a masonry quality index (M_l^{UR}) is the ratio between the length of the blue line traced only through the masonry joints following the structured path UP-RIGHT (v_l^{UR}) and the height of the RMPW (H_w)



(a)



(b)

Fig. 3. (a) Graphical interpretations of the lines of vertical trace (M_l^{UR} , M_l^{URUL} , M_l^{min}); (b) Synoptic representation of values assumed by the line of vertical traces for regular and non-regular patterns.

reading to:

$$M_l^{UR} = \frac{v_l^{UR}}{H_w} \tag{8}$$

However, such a path could be not practical in some cases since it might require a very wide RMPW to connect the upper and the lower edges. Therefore, within the scope to make such a formulation more appealing for real case studies, and consequently taking into account that in some situations, it is necessary the removal of the plaster in order to inspect the masonry pattern, an alternative masonry index, i.e., following a structured path UP-RIGHT-UP-LEFT, is proposed (see Fig. 3a second column):

$$M_l^{URUL} = \frac{v_l^{URUL}}{H_w} \tag{9}$$

Remark 2. M_l^{UR} and M_l^{URUL} are masonry indexes here defined. When regular masonry characterises the structure under investigation, M_l^{URUL} provides the same evaluation than M_l^{UR} as well as that of the lines of the minimum trace (M_l^{\min}), as defined in [60,61] (see Fig. 3a third column).

Remark 3. On the contrary, when the masonry pattern is coherent with Fig. 2b, the use of the line of minimum trace, will provide a lower value with respect to M_l^{UR} , since the algorithm will search at each node the shortest path to connect the upper and lower edges of the RMPW. Instead, the structured path UP-RIGHT-UP-LEFT (M_l^{URUL}) removes the underestimation generated by the use of the classical definition of the line of minimum trace (M_l^{\min}), providing an assessment very close to M_l^{UR} . Since both paths, i.e., UP-RIGHT-UP-LEFT and UP-RIGHT are pre-assigned, when the algorithm has to trace along the horizontal direction, there is a 50% chance of following the shortest or longest side resulting in $M_l^{UR} \simeq M_l^{URUL}$, in the case of an appropriate number of courses are considered.

In order to clarify these remarks, a synoptic representation of value assumed by M_l^{URUL} and M_l^{\min} with respect to the reference corresponding to the structured path UP-RIGHT (M_l^{UR}), for regular and non-regular coursed masonries, is represented in Fig. 3b.

Referring to both regular and non-regular patterns, M_l^{URUL} can be defined with the following equation:

$$M_l^{URUL} = \frac{\sum_{i=1}^{n_c} v_i}{\sum_{i=1}^{n_c+1} h_i} + 1 \tag{10}$$

where n_c is the number of courses, v_i and h_i are the horizontal interfaces' length and height of the unit blocks traced at the specific course.

Therefore, by assuming the equivalence between M_l^{URUL} and M_l^{UR} (see Fig. 3b) it is possible to manipulate Eq. (10) and Eq. (7) and solve for $\tan(\alpha_b)$:

$$\tan(\alpha_b) = (M_l^{URUL} - 1) \tag{11}$$

3.2. Rubble masonry

When the masonry has a rubble pattern, it is not possible to follow a structured path, i.e., UP-RIGHT-UP-LEFT or UP-RIGHT, since clear horizontal and vertical joints cannot be identified. Hence, whenever the masonry pattern appears chaotic, i.e., with blocks having various shapes and sizes and no evidence of horizontal courses, M_l^{\min} should be adopted in order to generate an analytical relationship between the masonry pattern typology and the crack inclination upper threshold. To accomplish the latter, for the specific RMPW, M_l^{\min} is assessed and then adopted to identify an equivalent regular masonry pattern, in which the equivalence is defined by assuming a regular pattern characterised by the same value of M_l^{\min} (Fig. 4). As a consequence, the crack inclination upper threshold defined in Eq. (11), is reformulated by replacing M_l^{URUL} with M_l^{\min} :

$$\tan(\alpha_b) = (M_l^{\min} - 1) \tag{12}$$

It is worth noting that the equivalence represented in Fig. 4 is developed considering that the masonry courses are perfectly horizontal (Fig. 4b), which is the ideal condition for unreinforced masonry structures providing uniform contact surfaces between units.

Remark 4. According to field and experimental observations reported in [60], the absence of horizontal joints influences masonry pattern capacity to generate frictional resistance, reducing the crack inclination upper threshold.

In order to better explain this concept, in Fig. 5 the frictional force is computed for the same column of material for both a horizontal interface and one characterised by an inclination of β . When the interface is inclined, the horizontal component of the frictional resistance,

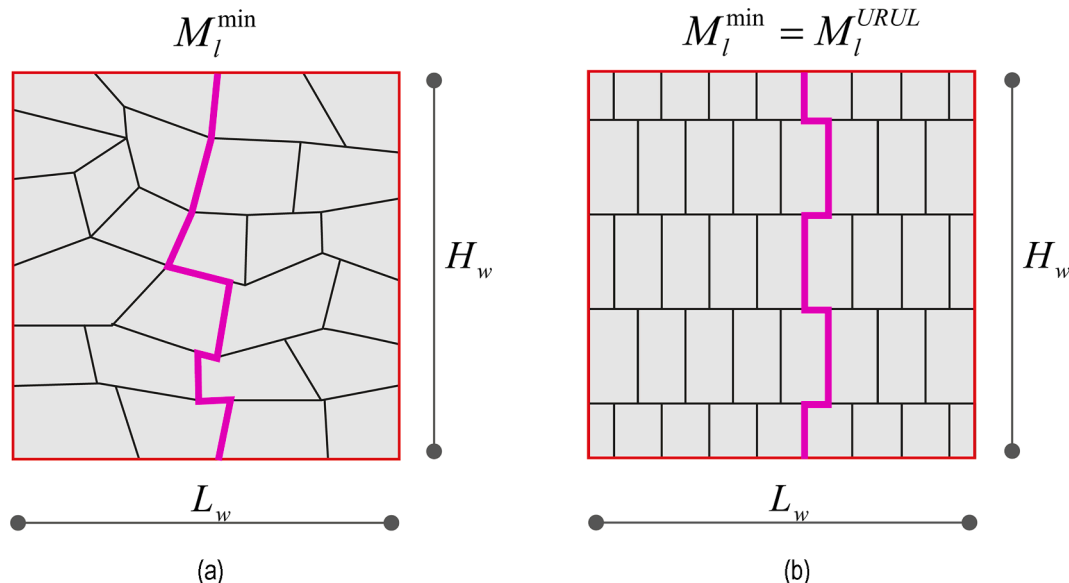


Fig. 4. Equivalence between rubble (a) and regular (b) patterns expressed in terms of M_l^{\min} .

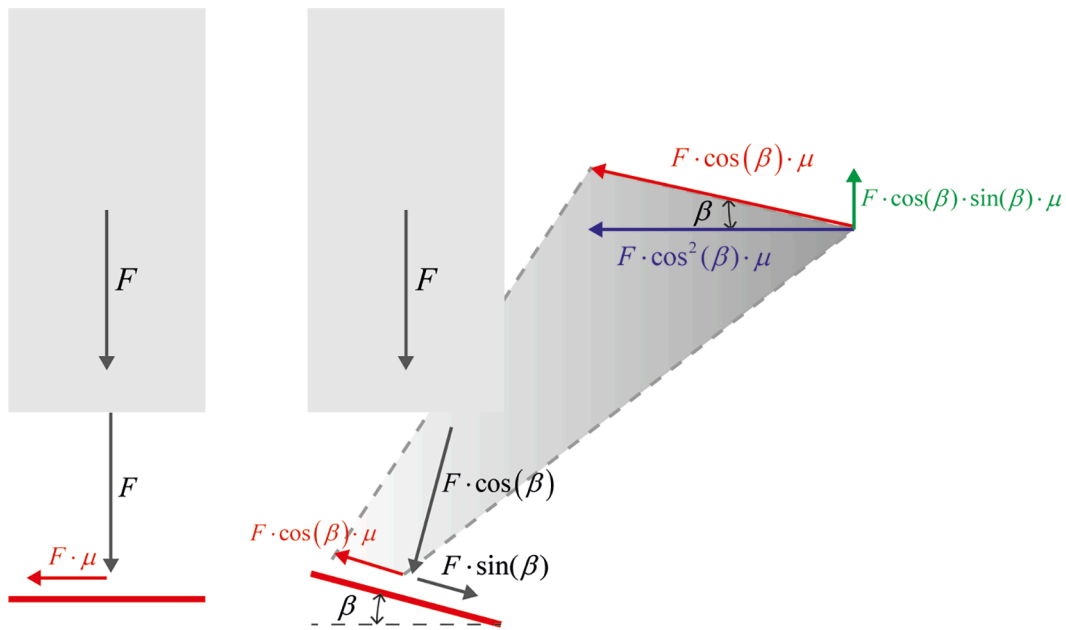


Fig. 5. Computation of the horizontal component of the frictional resistance in horizontal or inclined interfaces.

according to Coulomb’s law, is equal to $F \cdot \cos^2(\beta) \cdot \mu$, whereas, for the horizontal interface, it is equal to $F \cdot \mu$ (Fig. 5).

Referring again to the Coulomb’s frictional resistance generated by the in-plane wall depicted in Fig. 1, Eq. (3) underlines how α_b plays a role in the numerical evaluation of the frictional resistance. Keeping in mind what is represented in Fig. 5, in case of inclined interfaces, the user has to consider the horizontal component of the frictional resistance that requires the knowledge of the term $\cos^2(\beta)$. Hence, such a term might be introduced into Eq. (3) via the definition of the crack inclination upper threshold α_b , which his definition is the aim of the present formulation.

In order to take into account the uncoursed character of some masonry arrangements, here, the line of minimum trace (M_{Ol}) is defined as the ratio between the distance to connect two points located on the left and right boundaries of a given RMPW, passing only through joints and the horizontal distance between the two points (Fig. 6a):

$$M_{Ol} = \frac{v_{Ol}}{L_w} \tag{13}$$

Such a parameter assumes a value of $M_{Ol} = 1$ if perfect horizontal courses characterise the masonry pattern and $M_{Ol} > 1$ in the case of uncoursed masonry.

Fig. 6b shows a piecewise linear function $pl(l)$ that is representative of the traced line across the joints to evaluate M_{Ol} , and a continuous linear function $lc(l)$, which is characterised by the same length of the piecewise function ($v_{Ol} = \bar{v}_{Ol}$) and a constant slope which is computed as follows:

$$\tan(\bar{\beta}) = \frac{\sqrt{v_{Ol}^2 - L_w^2}}{L_w} \tag{14}$$

$\bar{\beta}$ assumes the physical meaning of an equivalent inclination of the

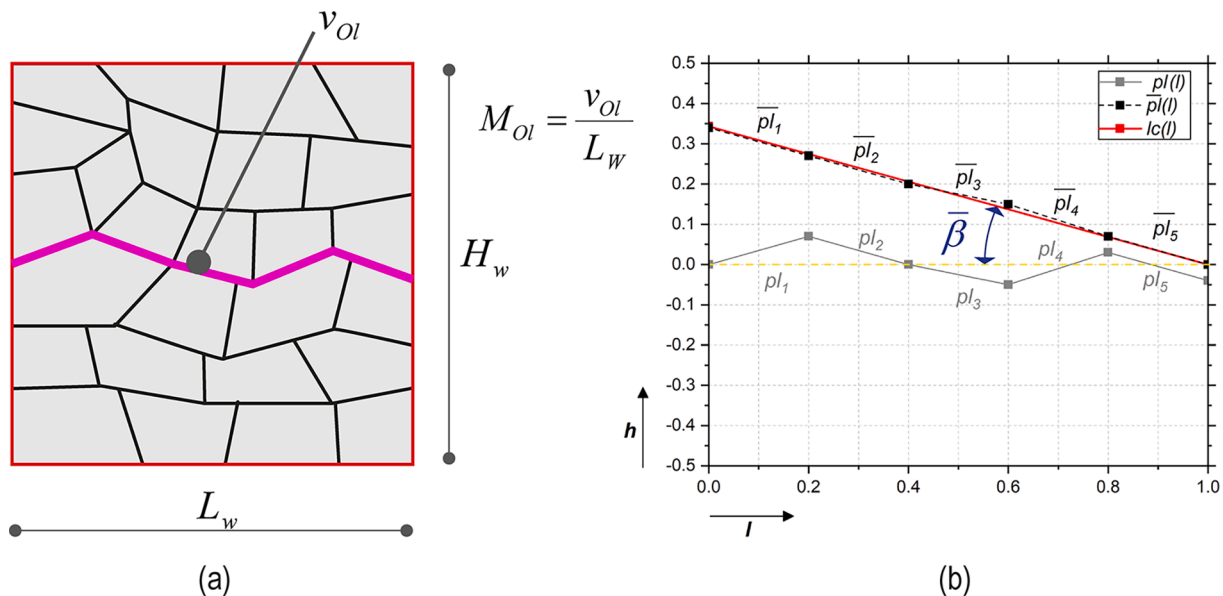


Fig. 6. Correction of frictional resistance taking pseudo-horizontal masonry joints orientation into account: (a) Graphical interpretation of the horizontal line of minimum length M_{Ol} ; (b) Graphical interpretation of the equivalent interface inclination ($\bar{\beta}$).

masonry interfaces, and Eq. (14) permits its approximate computation just by measuring v_{O_i} . Fig. 6 also shows how the $lc(l)$ function well simulates the transformed $pl(l) \rightarrow \bar{p}l(l)$, where in $\bar{p}l(l)$ all the pieces have the same length as $pl(l)$, but the absolute values of their own slopes are considered and joined in a continuous line.

One can note that the computation of the slope of each piece ($\beta_1, \beta_2, \dots, \beta_n$) and the consequent assessment of the horizontal frictional component appear more rigorous from the physical perspective but inevitably increases practitioners' difficulties.

Furthermore, the graphical construction reported in Fig. 6b, allows to define the following equivalence:

$$\cos(\bar{\beta}) = L_w / \bar{v}_{O_i} = 1 / M_{O_i} \quad (15)$$

Hence multiplying by $\cos^2(\bar{\beta})$ or dividing by $M_{O_i}^2$ is mathematically equivalent.

In order to take into consideration the lower frictional resistance generated by the inclined interfaces, the definition of the equivalent α_b reported in Eq. (12) gets to:

$$\tan(\alpha_b) = \frac{(M_l - 1)}{M_{O_i}^2} \quad (16)$$

Eq. (16) can be adopted for all the masonry typologies described in Sections 3.1 and 3.2, taking into consideration the following statements:

$$\begin{aligned} M_l &= M_l^{\min} \rightarrow \text{for rubble} \\ M_l &= M_l^{URUL} \rightarrow \text{for regular and non - regular coursed squared} \end{aligned} \quad (17)$$

Remark 5. As previously stated, the procedure implemented above provides an approximation in the computation of $\bar{\beta}$ but avoids the complication of individually decomposing $pl(l)$ in linear pieces and getting the slope of each piece.

Remark 6. According to Fig. 5, the weight of the material column also has a parallel component to the interface, i.e., $F \cdot \sin(\beta)$, that increases or decreases the actual frictional resistance component to the horizontal inertial actions, depending on the inclination of the interface. Similarly, the friction force computed for an inclined joint also has a vertical component that in turn, may perform stabilising or destabilising work if the slope is positive or negative, respectively. However, from the practical perspective, and considering any rubble masonry pattern, interfaces having positive or negative slopes may be considered equivalent in number and length. Consequently, these two contributions are considered close to zero and thus neglected in the proposed formulation.

4. Algorithm description

The previous sections described an analytical formulation to quantify the equivalent maximum admissible crack angle for different masonry typologies. The following section reports the detailed description of the algorithm to calculate the horizontal load factor and the corresponding failure mechanism.

After a visual inspection, the user can take a picture of the RMPW and perform its vectorisation within a software CAD. Once identified the masonry typology, e.g., according to the definition provided in Sections 3.1 and 3.2, α_b can be computed according to Eq. (16).

If one refers to rubble masonry, for defining M_l^{\min} , the user must trace the minimum distance to connect two points in the up and down edges of the selected windows, whereas M_{O_i} should be evaluated at each pseudo-course, and the maximum value, acting as a penalty factor for α_b has to be selected. On the contrary, if the structure under investigation is characterised by regular or non-regular coursed squared masonries, the structured path UP-RIGH-UP-LEFT drives the definition of the crack inclination upper threshold.

Once appropriately defined α_b , the constrained minimisation problem can be solved according to Eq. (5). Such a constrained optimisation

problem has been mathematically implemented in a GHPython script [63,65]. The solution is achieved using a heuristic solver based on the Nelder-Mead method [66] that is able to refine the geometry of the macroblocks and search for the minimum value of the load multiplier λ within a few seconds. A schematic presentation of the algorithm is reported in Table 1.

5. Brief DEM description

This study uses the discrete element method (DEM) formulated for rigid bodies to validate the proposed LA framework. The employed discontinuum-based approach was developed by Cundall [67] and extensively used to simulate the quasi-static and dynamic behaviour of masonry structures in the literature for the last several decades [68–70].

Briefly, the numerical procedure of DEM relies on the integration of translational and rotational equations of motion to predict the movements of distinct blocks along with their mechanical interactions with each other. The numerical solutions of the governing differential equations are obtained using the central difference method, in which the velocities are evaluated at the mid-intervals of the time step (Δt , $t^+ = t + \Delta t/2$, $t^- = t - \Delta t/2$). The explicit formulation of the equations of motion (written for the centre of mass of an undamped rigid body) is given in Eq. (18) and Eq. (19), respectively for translation and rotation. Note that each rigid block, indicated by the subscript i , has six degrees of freedom: 3 translational and 3 rotational in the three-dimensional space.

$$\dot{u}_i^{t+} = \dot{u}_i^{t-} + \sum F_i^t \frac{\Delta t}{m} \quad (18)$$

$$\dot{\omega}_i^{t+} = \dot{\omega}_i^{t-} + \sum M_i^t \frac{\Delta t}{I} \quad (19)$$

where \dot{u} , $\dot{\omega}$, m and I are the translational and angular velocity vectors, block mass and moment of inertia. Furthermore, $\sum F_i^t$ and $\sum M_i^t$ denote the unbalanced force vector, including the sum of the contact forces, self-weight, and applied forces, and moment vector consisting of the sum of moments produced by contact and applied forces, respectively. The quasi-static solutions are obtained from the given dynamic equations by adopting Cundall's local damping formulation [71]. The new velocities (\dot{u}_i^{t+} , $\dot{\omega}_i^{t+}$) are further utilised to update rigid block position and relative contact displacements (Δu_n , Δu_s). The contact forces are computed via the linear/nonlinear springs defined in the normal and shear directions depending on the relative contact displacements (Fig. 7). In this study, linear compression behaviour (no failure) with zero-tensile strength is considered to simulate dry-joint masonry behaviour in the normal direction, whereas the Coulomb-slip joint model is employed in the shear direction, requiring initial and residual friction coefficients (μ_0 , μ_{res}), shown in Fig. 7. Through the explicit solution scheme of DEM, contact conditions are constantly monitored via a contact detection algorithm based on the common plane concept, explained in [72]. Therefore, possible failure modes such as joint opening, sliding, and total contact loss are captured during the analysis.

Table 1
Description of the proposed method.

Start
Visual inspection
Identification of the masonry typology
compute $\tan(\alpha_b) = \frac{(M_l - 1)}{M_{O_i}^2}$
if masonry typology is regular and non-regular coursed squared, assume $M_l = M_l^{URUL}$
if masonry typology is rubble, assume $M_l = M_l^{\min}$
Parametrisation of the failure mechanism
Define the equilibrium equation according to the virtual work principle (Eq. (1))
Solve the constrain minimisation problem according to Eq. (5)
Get horizontal load factor and associated macro-block failure mechanism
End

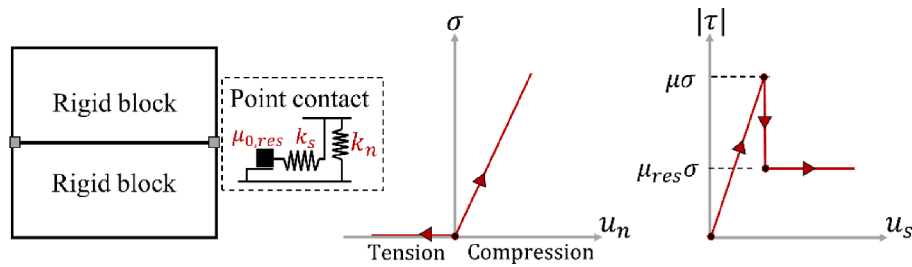


Fig. 7. Illustration of point contact and defined contact constitutive laws in normal and shear directions.

The normal and shear contact stresses (denoted as σ and τ , respectively) are calculated as elastic trials in an incremental format ($\Delta\sigma = k_n\Delta u_n$, $\Delta\tau = k_s\Delta u_s$) and added to the previous ones that are updated (if applicable) based on the adopted stress-displacement criteria. Finally, new contact stresses are multiplied with the associated contact area and included in the unbalanced force and moment equations to predict the new velocities as given earlier in Eqs. (18) and (19).

The time-step Δt is adjusted to ensure numerical stability during the analysis since the central difference method provides only conditionally stable solutions. A commercial discrete element code, 3DEC developed by Itasca, is used throughout this research, which automatically provides a critical time step. Simply, the critical time step (Δt_c) is determined based on the minimum block mass (m_{min}) and maximum contact stiffness ($k_{n,max}$) in the discrete block system ($\Delta t_c = 0.2\sqrt{m_{min}/k_{n,max}}$).

Hence, the mechanical behaviour of dry-joint masonry walls is simulated by a system of rigid blocks following the dynamic solution cycle of DEM, as explained in this section. Next, the applications of DEM-based simulations are presented and compared with the LA.

6. Validation by comparing LA and DEM results

The proposed analytical model is verified by investigating a number of case studies compared to advanced DEM simulations and numerical results arising from the literature. The first step in the validation scheme involves two sets of shear walls (each set is comprised of three masonry patterns characterised by an increasing degree of randomness). The masonry patterns used the generator available in Grasshopper plugin for Rhinoceros [63]. Finally, three real case studies of churches located in central Italy have been simulated, and results are compared with those reported in de Felice et al. [73].

6.1. In-plane shear walls

These numerical simulations aim at verifying the capability of the proposed LA framework to predict the geometry of the collapse mechanism and the horizontal capacity of in-plane shear walls characterised by different masonry patterns ranging from regular and periodic to non-periodic. The analysed masonry patterns are illustrated in Fig. 8. Here, SET-1 is characterised by unit aspect ratio $m = v/h = 0.75$, whereas SET-2 is characterised by unit aspect ratio $m = 0.50$. Also, case (a) is regular, case (b) is affected by courses having random heights and case (c) is non-periodic.

In DEM simulations, the loading condition is idealised in two steps: i) equilibrium is obtained under gravity; ii) then a lateral acceleration field is defined, which is gradually increased until failure mechanism is reached. The mechanical properties utilised in discrete element models to simulate dry-joint masonry walls are listed in Table 2.

Fig. 8 also represents the selection of three different RMPW adopted to evaluate the practical engineering parameters needed to apply the proposed analytical formulations, i.e., M_I and M_{O_I} . Finally, Table 3 summarises the values of M_I and M_{O_I} for all the simulated shear walls.

In Fig. 9, a comparison in terms of the load–displacement curve between the proposed analytical model and the DEM simulations is represented. The lateral forces, proportional to mass, are prescribed in

Table 2 Mechanical properties adopted in DEM simulations.

k_n [GPa/m]	k_s [GPa/m]	ρ [kg m ⁻³]	μ [-]
1.0	0.4	2000	0.70

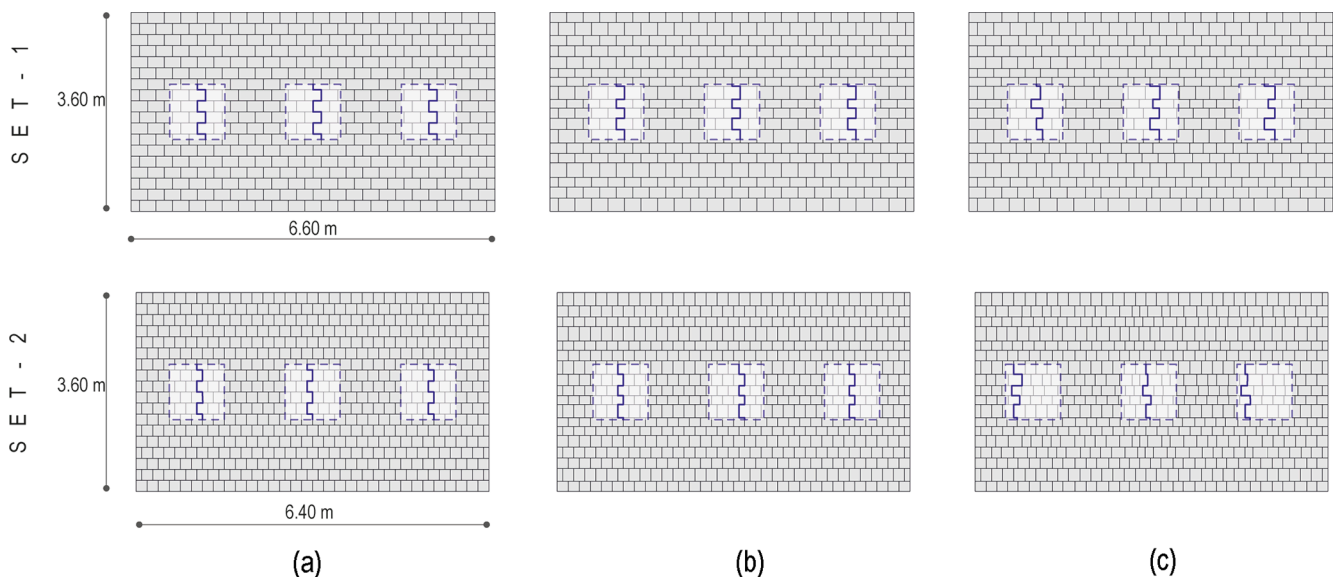


Fig. 8. Shear-wall prototypes: SET-1 and SET-2.

Table 3
Computation of M_I and M_{OI} for the structures under investigation.

	SET-1			SET-2		
	a	b	c	a	b	c
M_I	1.75	1.75	$1.75 \pm 5\%$	1.50	1.50	$1.53 \pm 7\%$
M_{OI}	1.00	1.00	1.00	1.00	1.00	1.00

discrete element models, gradually increasing until reaching failure. The blocks participating in the collapse mechanism are determined once no quasi-static equilibrium is found in the computational model and the

group of blocks reveals unbounded displacement under the given loading condition. Accordingly, the ultimate displacement is obtained based on the collapse mechanism and the associated turning point of the macro-block. LA results are reported for each representative RMPW reported in Fig. 8 involving in enveloped results the represented envelops. The proposed LA framework demonstrates its ability to carefully estimate the structural capacity of both periodic (SET-1a and SET-2a) and non-periodic masonry structures (SET-1b,c and SET-2b,c). This holds for maximum acceleration (or force capacity) and maximum displacement. Referring to the LA results, one should note that the loading displacement curves have been simplified with a linear

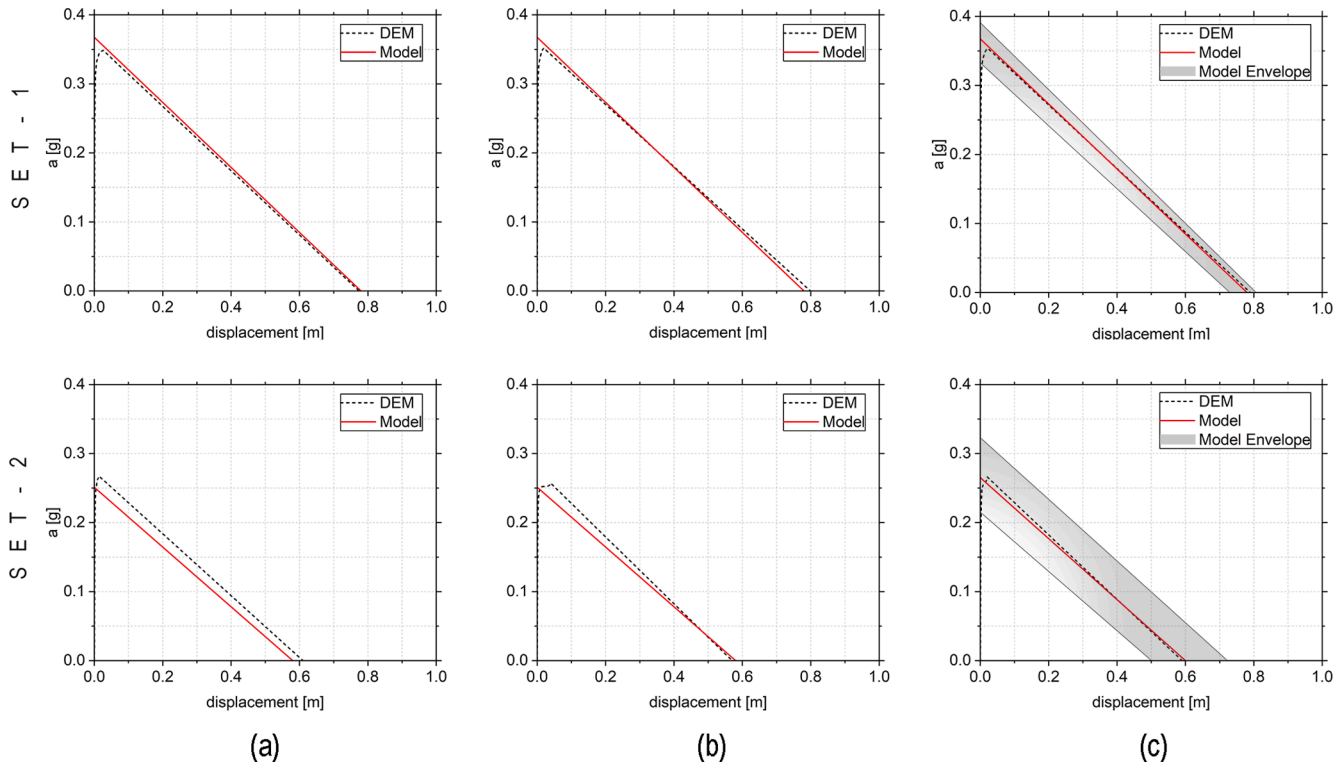


Fig. 9. Pushover curves, measuring applied horizontal acceleration vs horizontal displacement of the left corner: (a) regular; (b) curves having random heights; (c) non-periodic.

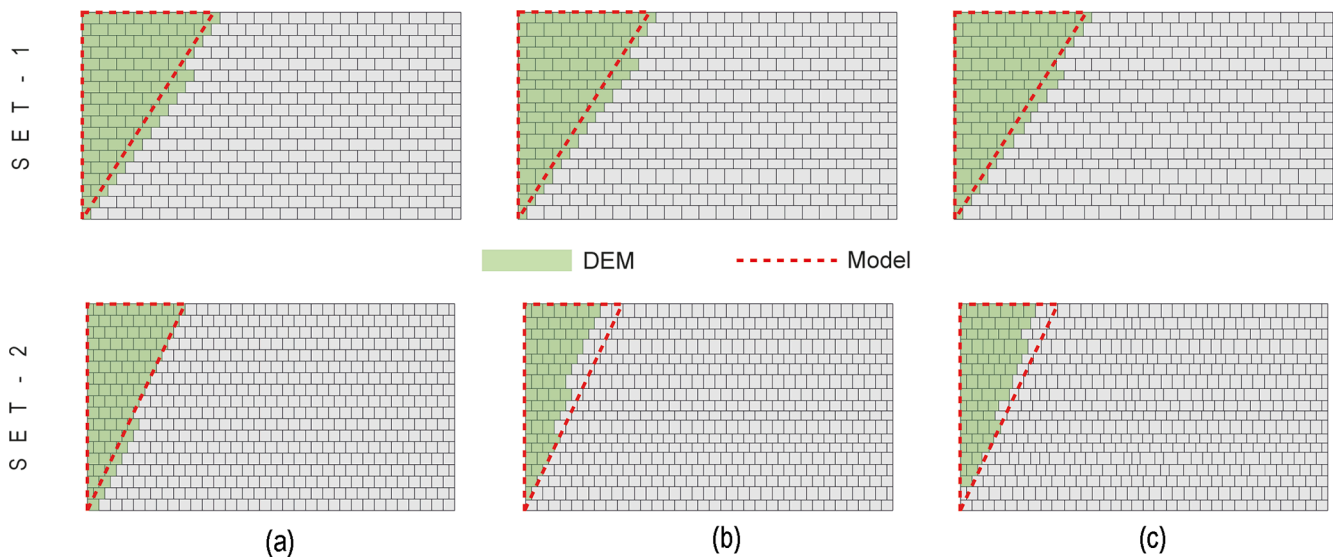


Fig. 10. Comparison in terms of predicted failure mechanisms: DEM vs Model (a) regular; (b) curves having random heights; (c) non-periodic.

descending branch. However, for the sake of rigour, the procedure proposed in [74] should be adopted, where the authors considered the actual interfaces' capability to generate frictional resistance during the loading history.

Regarding the collapse mechanisms, Fig. 10 compares the geometry of the failure mechanisms between DEM (shaded in green) and the proposed LA framework (defined as a red triangle). There is an evident good agreement between the macroblock detected by the proposed model and the blocks involved in the collapse mechanisms obtained with DEM. The obtained results in terms of the loading displacement curves and collapse mechanisms demonstrate the adequacy of the proposed analytical model.

7. Case studies: Churches in central Italy

In this section, the proposed analytical model is applied to three single-nave churches belonging to the area surrounding the city of L'Aquila [73]. The churches under investigation are named: Church of S. Maria del Presepe (C1), Church S. Maria degli Angeli (C2) and Church S. Maria ad Cryptas (C3). The churches are analysed in a 2D framework, being the third dimension considered by providing the parts' thickness according to the sketch reported in Fig. 11a. Table 4 lists the geometrical characteristics of the churches, which are schematically represented in Fig. 11. Furthermore, Fig. 11b-d represents the real masonry patterns adopted for the simulation, which the authors [73] kindly provided to conduct the present research work. In the same sketches, the RMPWs adopted to evaluate M_l and M_{Ol} are shown in white shading. These values are also listed in Table 4. The friction coefficient is taken constant for all the churches under investigation ($\mu = 0.57$).

The comparisons in terms of load–displacement curves are reported in Fig. 12, where the pushover curves regarding C1, C2 and C3 are represented in Fig. 12a, b and c, respectively. The proposed analytical model and DEM simulations from [63] have an excellent agreement in terms of both capacity and ultimate displacement. On the contrary, the Rigid Block (RB) model [73], accounting only for the façade overturning, always underestimate both structural capacity in terms of force

and ultimate displacement of the structures under investigation.

Fig. 13 confirms the effectiveness of the proposed analytical model in terms of the predicted failure mechanism. The proposed model is able to adequately simulate the crack inclination across the sidewalls, which are characterised by rubble masonry patterns. In terms of the identification of the failure mechanism, the small difference between DEM and LA approaches derives from the fact that in de Felice et al. [73], the authors only considered the rocking blocks and did not consider the blocks sliding in the failure mechanism, while in the LA the boundary of the failure mechanism is somewhere in between the rocking and the sliding failure line. Furthermore, in the case of the C2 and C3, the LA approach neglects the presence of the small openings. The investigation of the openings is out of the scope of this research work and will be investigated in future works.

8. Conclusions

This paper ambitiously presents a new formulation to assess the frictional resistance adopted in a macro-block LA formulation for historic masonry structures, specifically for the in-plane sliding-rocking failure mechanism. Such an approach takes advantage by the knowledge of practical engineering parameters, i.e., vertical and horizontal lines of minimum trace, for computing the frictional resistance in different masonry typologies. Compared with existing macro-block formulations for the in-plane rocking-sliding failure mechanism, the proposed analytical model introduces the concept of RMPW for the definition of the frictional resistance. Specifically, in [55,59], which accounts for regular masonry patterns, the single unit blocks aspect ratio is adopted to evaluate the frictional resistance. On the contrary, when different masonry typology characterises the structure under investigation, an RMPW should be identified, and the proposed procedure applied accordingly.

As a result, the analytical model can provide an estimation of the lateral capacity of a range of different masonry walls and an accurate prediction of the geometry of the macro-block involved in the failure mechanism. A refined DEM modelling has been adopted as a reference

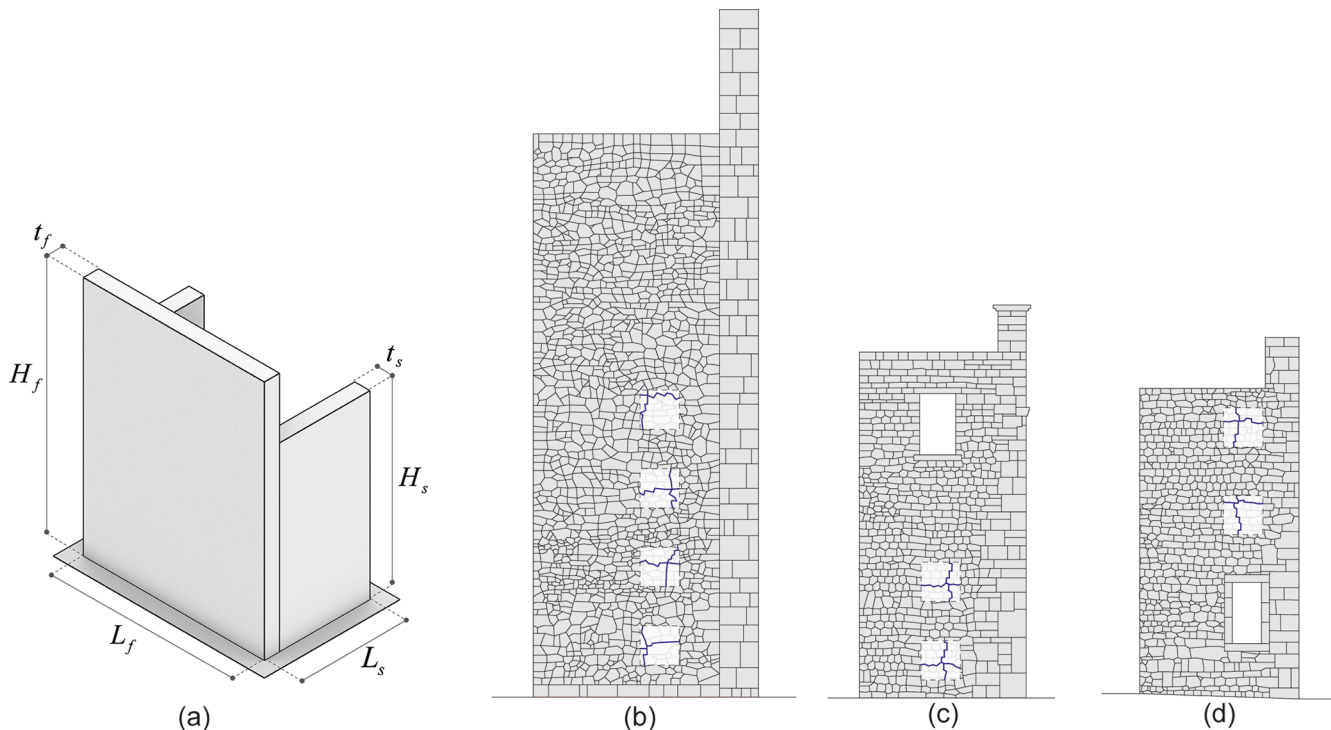


Fig. 11. Churches under investigation: (a) geometrical configuration; (b) Church of S. Maria del Presepe (C1); (c) Church S. Maria degli Angeli (C2); (d) Church S. Maria ad Cryptas (C3).

Table 4
Geometrical properties and densities of the churches under investigation.

	Façade			ρ [kg m ⁻³]	Side wall		ρ [kg m ⁻³]	Vert. length	Hor. Length
	L_f [m]	t_f [m]	h_f [m]		t_s [m]	h_s [m]		M_l [-]	M_{ol} [-]
C1	9.95	0.75	13.30	2200	1.40	10.40	2100	1.18 ± 7%	1.18 ± 5%
C2	10.00	0.70	10.00	2100	0.50	8.80	2000	1.31	1.08
C3	10.20	0.86	9.50	2100	1.00	7.90	2100	1.24	1.12

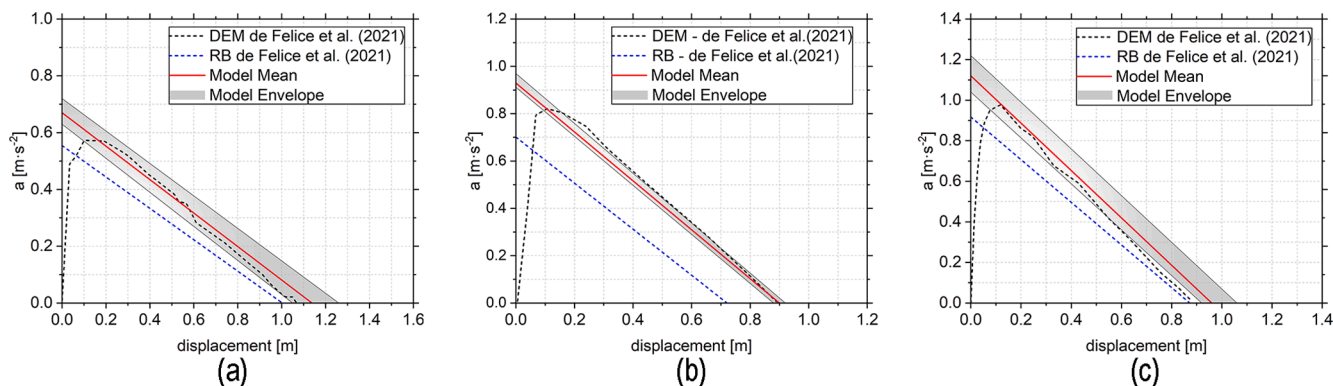


Fig. 12. Pushover curves, measuring applied horizontal acceleration vs horizontal displacement: (a) Church of S. Maria del Presepe (C1); (b) Church S. Maria degli Angeli (C2); and (c) Church S. Maria ad Cryptas (C3).

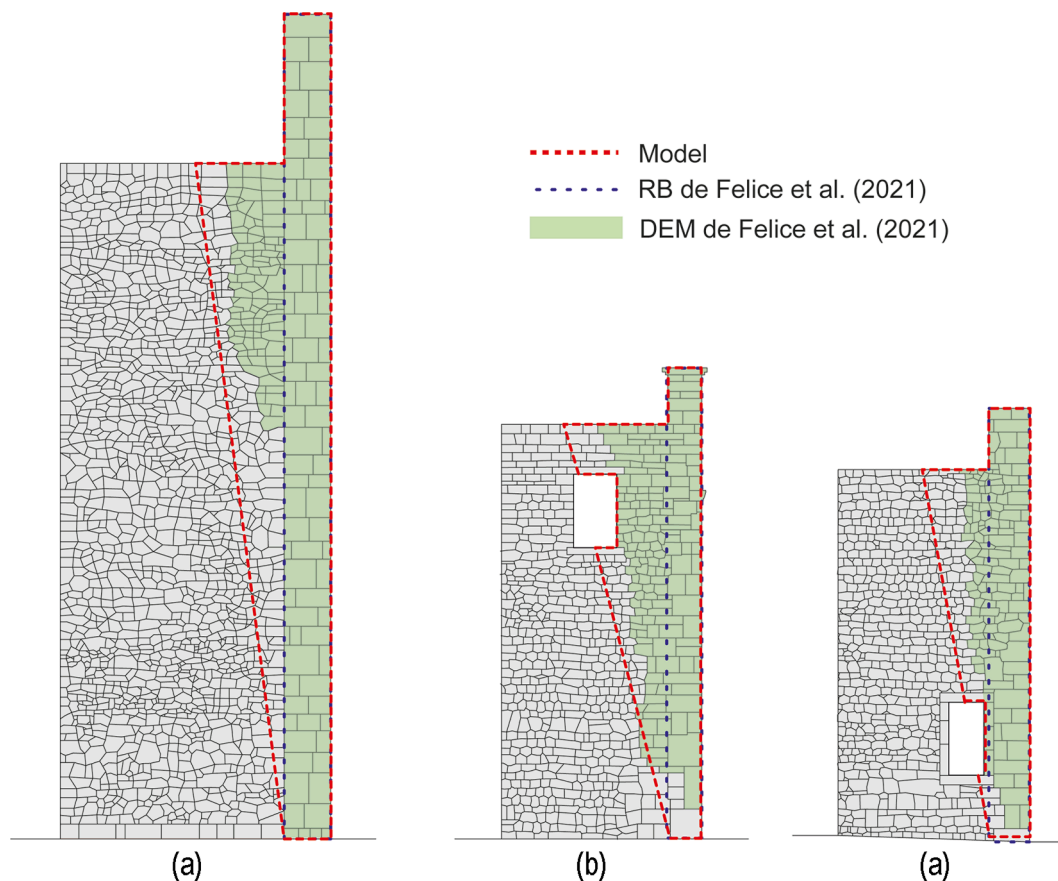


Fig. 13. Comparison in terms of predicted failure mechanisms: DEM and RB vs Model (a) Church of S. Maria del Presepe (C1), (b) Church S. Maria degli Angeli (C2), and (c) Church S. Maria ad Cryptas (C3).

model for the validation of the proposed approach. Furthermore, cases of study have been investigated (shear walls and churches in central Italy), and the results compared with the refined DEM models. The following points summarise the main findings and contributions of the paper:

- The proposed analytical model uses the definition of easy detectable geometrical parameters, i.e., vertical and horizontal lines of minimum length.
- The analytical model is totally independent from mechanical parameters (as it is only based on the knowledge of some masonry quality indexes, except the friction coefficient) and does not require computational power to get results, making this tool particularly suitable for the assessment of a considerable number of structures in no time.
- The proposed analytical model can assess the structural performance of walls characterised by different masonry patterns in a given wall, which occurs in several historical masonry structures subjected to modification over the centuries or reconstruction after damage induced by past earthquake events.
- The use of masonry indexes to classify masonry typologies and assess mechanical properties will open new perspectives within the probabilistic assessment of historic masonry structures, which is the objective of the work currently being developed by the authors.

Future developments will involve: i) the adoption of the proposed approach for the territorial scale assessment of masonry buildings characterised by different masonry textures; ii) parametrisation of other locale failure mechanisms; iii) implementation of a proper segmentation algorithm able to estimate the value of masonry quality indexes just by taking pictures avoiding time-consuming vectorisation of the masonry texture [75,76].

CRediT authorship contribution statement

Marco Francesco Funari: Conceptualization, Methodology, Validation, Visualization, Writing – original draft. **Bora Pulatsu:** Validation, Writing – original draft. **Simon Szabó:** Conceptualization, Validation, Writing – original draft. **Paulo B. Lourenço:** Funding acquisition, Supervision, Writing – review & editing.

Declaration of Competing Interest

The authors declare that they have no known competing financial interests or personal relationships that could have appeared to influence the work reported in this paper.

Acknowledgements

The authors want to gratefully acknowledge Professor Gianmarco de Felice, Dr Francesca Gobbin and Rebecca Fugger, at Roma Tre University, Italy, for kindly sharing the masonry patterns of the churches S. Maria del Presepe, S. Maria degli Angeli, and S. Maria ad Cryptas [74].

Funding

This work was partly financed by FCT/MCTES through national funds (PIDDAC) under the R&D Unit Institute for Sustainability and Innovation in Structural Engineering (ISISE), under reference UIDB/04029/2020. This study has been partly funded by the STAND4-HERITAGE project (New Standards for Seismic Assessment of Built Cultural Heritage) that has received funding from the European Research Council (ERC) under the European Union's Horizon 2020 research and innovation programme (Grant agreement No. 833123), as an Advanced Grant.

References

- [1] Lourenço PB. The ICOMOS methodology for conservation of cultural heritage buildings: Concepts, research and application to case studies. REHAB 2014 - Proc Int Conf Preserv Maint Rehabil Hist Build Struct, Green Lines Institute for Sustainable Development; 2014, p. 945–54. <https://doi.org/10.14575/gl/rehab2014/095>.
- [2] Milić M, Stepinac M, Lulić L, Ivanišević N, Matorić I, Šipoš BČ, et al. Assessment and rehabilitation of culturally protected prince Rudolf infantry barracks in Zagreb after major earthquake. *Build* 2021;11:508. <https://doi.org/10.3390/BUILDINGS11110508>.
- [3] Stepinac M, Lourenço PB, Atalić J, Kisiček T, Uroš M, Baniček M, et al. Damage classification of residential buildings in historical downtown after the ML5.5 earthquake in Zagreb, Croatia in 2020. *Int J Disaster Risk Reduct* 2021;56:102140.
- [4] D'Altri AM, Sarhosis V, Milani G, Rots J, Cattari S, Lagomarsino S, et al. Modeling strategies for the computational analysis of unreinforced masonry structures: Review and classification. *Arch Comput Methods Eng* 2020;27(4):1153–85. <https://doi.org/10.1007/s11831-019-09351-x>.
- [5] Karimzadeh S, Kadas K, Askan A, Erberik MA, Yakut A. Derivation of analytical fragility curves using SDOF models of masonry structures in Erzincan (Turkey). *Earthquakes Struct* 2020;18:249–61.
- [6] Sarhosis V, Milani G, Formisano A, Fabbrocino F. Evaluation of different approaches for the estimation of the seismic vulnerability of masonry towers. *Bull Earthq Eng* 2018;16(3):1511–45.
- [7] Giordano A, Mele E, De Luca A. Modelling of historical masonry structures: comparison of different approaches through a case study. *Eng Struct* 2002;24(8):1057–69.
- [8] Fortunato G, Funari MF, Lonetti P. Survey and seismic vulnerability assessment of the Baptistery of San Giovanni in Tumba (Italy). *J Cult Herit* 2017;26:64–78. <https://doi.org/10.1016/j.culher.2017.01.010>.
- [9] Szabó S, Kövesdi A, Vasáros Z, Csicsely Á, Hegyi D. The cause of damage and failure of the Mud-brick vault of the Khan in New-Gourna. *Eng Fail Anal* 2021;128:105567. <https://doi.org/10.1016/j.engfailanal.2021.105567>.
- [10] Funari MF, Hajjat AE, Masciotta MG, Oliveira DV, Lourenço PB. A parametric scan-to-FEM Framework for the digital twin generation of historic masonry structures. *Sustainability* 2021;3:11088. <https://doi.org/10.3390/SU131911088>.
- [11] Hoveidae N, Fathi A, Karimzadeh S. Seismic damage assessment of a historic masonry building under simulated scenario earthquakes: a case study for Arge-Tabriz. *Soil Dyn Earthq Eng* 2021;147:106732. <https://doi.org/10.1016/j.soildyn.2021.106732>.
- [12] Roca P, Cervera M, Pelà L, Clemente R, Chiumenti M. Continuum FE models for the analysis of Mallorca Cathedral. *Eng Struct* 2013;46:653–70. <https://doi.org/10.1016/j.engstruct.2012.08.005>.
- [13] -> Valente M, Milani G. Non-linear dynamic and static analyses on eight historical masonry towers in the North-East of Italy. *Eng Struct* 2016;114:241–70.
- [14] Milani G, Valente M, Fagone M, Rotunno T, Alessandri C. Advanced non-linear numerical modeling of masonry groin vaults of major historical importance: St John Hospital case study in Jerusalem. *Eng Struct* 2019;194:458–76. <https://doi.org/10.1016/j.engstruct.2019.05.021>.
- [15] Lemos JV. Discrete element modeling of masonry structures. *Int J Archit Herit* 2007;1:190–213. <https://doi.org/10.1080/15583050601176868>.
- [16] Lemos J. Discrete element modeling of the seismic behavior of masonry construction. *Buildings* 2019;9(2):43.
- [17] Bui TT, Limam A, Sarhosis V, Hjiat M. Discrete element modelling of the in-plane and out-of-plane behaviour of dry-joint masonry wall constructions. *Eng Struct* 2017;136:277–94. <https://doi.org/10.1016/j.engstruct.2017.01.020>.
- [18] Gonen S, Pulatsu B, Erdogmus E, Karaesmen E, Karaesmen E. Quasi-static nonlinear seismic assessment of a fourth century A.D. Roman Aqueduct in Istanbul, Turkey. *Heritage* 2021;4:401–21. <https://doi.org/10.3390/heritage4010025>.
- [19] Kim J, Lorenzoni F, Salvalaggio M, Valluzzi MR. Seismic vulnerability assessment of free-standing massive masonry columns by the 3D Discrete Element Method. *Eng Struct* 2021;246:113004. <https://doi.org/10.1016/j.engstruct.2021.113004>.
- [20] Savalle N, Lourenço PB, Milani G. Joint stiffness influence on the first-order seismic capacity of dry-joint masonry structures: numerical DEM investigations. *Appl Sci* 2022;12:2108.
- [21] Gálvez F, Ip K, Vaculik J, Griffith M, Sorrentino L, Dizhur D, et al. Discrete element modelling to predict failure strength of unreinforced masonry walls. *Proc Aust Earthq Eng Soc 2017 Conf* 2017.
- [22] da Silva L, Milani G. A FE-based macro-element for the assessment of masonry structures: linear static, vibration, and non-linear cyclic analyses. *Appl Sci* 2022;12:1248.
- [23] Gonen S, Soyoz S. Reliability-based seismic performance of masonry arch bridges. *Struct Infrastruct Eng* 2021;1–16. <https://doi.org/10.1080/15732479.2021.1918726>.
- [24] Savalle N, Vincens E, Hans S. Pseudo-static scaled-down experiments on dry stone retaining walls: preliminary implications for the seismic design. *Eng Struct* 2018;171:336–47. <https://doi.org/10.1016/j.engstruct.2018.05.080>.
- [25] Meriggi P, de Felice G, De Santis S, Gobbin F, Mordanova A, Pantò B. Distinct element modelling of masonry walls under out-of-plane seismic loading. *Int J Archit Herit* 2019;13(7):1110–23.
- [26] Malomo D, DeJong MJ, Penna A. Distinct element modelling of the in-plane cyclic response of URM walls subjected to shear-compression. *Earthq Eng Struct Dyn* 2019;48:1322–44. <https://doi.org/10.1002/eqe.3178>.
- [27] Simon J, Bagi K. Discrete element analysis of the minimum thickness of oval masonry domes. *Int J Archit Herit* 2016;10:457–75. <https://doi.org/10.1080/15583058.2014.996921>.

- [28] Sarhosis V, Lemos JV. A detailed micro-modelling approach for the structural analysis of masonry assemblages. *Comput Struct* 2018;206:66–81. <https://doi.org/10.1016/j.compstruc.2018.06.003>.
- [29] Pulatsu B, Erdogmus E, Lourenço PB, Quey R. Simulation of uniaxial tensile behavior of quasi-brittle materials using softening contact models in DEM. *Int J Fract* 2019;217:105–25. <https://doi.org/10.1007/s10704-019-00373-x>.
- [30] Ravi Prakash P, Pulatsu B, Lourenço PB, Azenha M, Pereira JM. A meso-scale discrete element method framework to simulate thermo-mechanical failure of concrete subjected to elevated temperatures. *Eng Fract Mech* 2020;239:107269. <https://doi.org/10.1016/j.engfracmech.2020.107269>.
- [31] Pulatsu B, Erdogmus E, Lourenço PB, Lemos JV, Hazzard J. Discontinuum analysis of the fracture mechanism in masonry prisms and wallets via discrete element method. *Meccanica* 2020;55:505–23. <https://doi.org/10.1007/s11012-020-01133-1>.
- [32] Galvez F, Sorrentino L, Dizhur D, Ingham JM. Using DEM to investigate boundary conditions for rocking URM facades subjected to earthquake motion. *J Struct Eng* 2021;147:04021191. [https://doi.org/10.1061/\(asce\)st.1943-541x.0003171](https://doi.org/10.1061/(asce)st.1943-541x.0003171).
- [33] Lemos JV, Sarhosis V. Discrete element bonded-block models for detailed analysis of masonry. *Infrastructures* 2022;7:31. <https://doi.org/10.3390/infrastructures7030031>.
- [34] Lourenço PB, Silva LC. Computational applications in masonry structures: From the meso-scale to the super-large/super-complex. *Int J Multiscale Comput Eng* 2020;18:1–30. <https://doi.org/10.1615/IntJMultCompEng.2020030889>.
- [35] Funari MF, Silva LC, Savalle N, Lourenço PB. A concurrent micro/macro FE-model optimized with a limit analysis tool for the assessment of dry-joint masonry structures. *Int J Multiscale Comput Eng* 2022. <https://doi.org/10.1615/IntJMultCompEng.2021040212>.
- [36] Malomo D, DeJong MJ. A Macro-Distinct Element Model (M-DEM) for simulating the in-plane cyclic behavior of URM structures. *Eng Struct* 2021;227:111428. <https://doi.org/10.1016/j.engstruct.2020.111428>.
- [37] D'Altri AM, Lo Presti N, Grillanda N, Castellazzi G, de Miranda S, Milani G. A two-step automated procedure based on adaptive limit and pushover analyses for the seismic assessment of masonry structures. *Comput Struct* 2021;252:106561. <https://doi.org/10.1016/j.compstruc.2021.106561>.
- [38] Vadalà F, Cusmano V, Funari MF, Caliò I, Lourenço PB. On the use of a mesoscale masonry pattern representation in discrete macro-element approach. *J Build Eng* 2022;50:104182. <https://doi.org/10.1016/j.jobe.2022.104182>.
- [39] Cascini L, Gagliardo R, Portioli F. LiABlock 3D: a software tool for collapse mechanism analysis of historic masonry structures. *Int J Archit Herit* 2020;14:75–94. <https://doi.org/10.1080/15583058.2018.1509155>.
- [40] De Felice G, Giannini R. Out-of-plane seismic resistance of masonry walls. *J Earthq Eng* 2001;5:253–71. <https://doi.org/10.1080/13632460109350394>.
- [41] Funari MF, Silva LC, Mousavian E, Lourenço PB. Real-time structural stability of domes through limit analysis: application to St. Peter's Dome. *Int J Archit Herit* 2021;1–23. <https://doi.org/10.1080/15583058.2021.1992539>.
- [42] Vaculik J, Griffith MC, Magesen G. Dry stone masonry walls in bending—part II: analysis. *Int J Archit Herit* 2014;8(1):29–48.
- [43] Nodargi NA, Bisegna P. A finite difference method for the static limit analysis of masonry domes under seismic loads. *Meccanica* 2022;57(1):121–41.
- [44] Livesley RK. Limit analysis of structures formed from rigid blocks. *Int J Numer Methods Eng* 1978;12(12):1853–71.
- [45] Ferris MC, Tin-Loi F. Limit analysis of frictional block assemblies as a mathematical program with complementarity constraints. *Int J Mech Sci* 2001;43(1):209–24.
- [46] Gilbert M, Casapulla C, Ahmed HM. Limit analysis of masonry block structures with non-associative frictional joints using linear programming. *Comput Struct* 2006;84(13–14):873–87.
- [47] Cascini L, Gagliardo R, Portioli F. LiABlock 3D: a software tool for collapse mechanism analysis of historic masonry structures. *Int J Archit Herit* 2020;14(1):75–94.
- [48] Portioli F, Casapulla C, Gilbert M, Cascini L. Limit analysis of 3D masonry block structures with non-associative frictional joints using cone programming. *Comput Struct* 2014;143:108–21. <https://doi.org/10.1016/J.COMPSTRUC.2014.07.010>.
- [49] Vaculik J, Griffith MC. Out-of-plane load-displacement model for two-way spanning masonry walls. *Eng Struct* 2017;141:328–43.
- [50] Mordà N, Mancini A. Norme tecniche per le costruzioni (NTC 2018) D. Min. Infrastrutture e Trasporti 17 gennaio 2018 2018.
- [51] Giuffrè A. A Mechanical Model for Statics and Dynamics of Historical Masonry Buildings. *Prot Archit Herit Against Earthquakes*, Springer Vienna; 1996, p. 71–152. https://doi.org/10.1007/978-3-7091-2656-1_4.
- [52] Funari MF, Spadea S, Lonetti P, Fabbrocino F, Luciano R. Visual programming for structural assessment of out-of-plane mechanisms in historic masonry structures. *J Build Eng* 2020;31:101425.
- [53] Casapulla C, Cascini L, Portioli F, Landolfo R. 3D macro and micro-block models for limit analysis of out-of-plane loaded masonry walls with non-associative Coulomb friction. *Meccanica* 2014;49(7):1653–78.
- [54] D'Ayala D, Speranza E. Definition of collapse mechanisms and seismic vulnerability of historic masonry buildings. *Earthq Spectra* 2003;19:479–509. <https://doi.org/10.1193/1.1599896>.
- [55] Funari MF, Mehrotra A, Lourenço PB. A tool for the rapid seismic assessment of historic masonry structures based on limit analysis optimisation and rocking dynamics. *Appl Sci* 2021;11:942. <https://doi.org/10.3390/app11030942>.
- [56] Funari MF, Spadea S, Ciantia M, Lonetti P, Greco F. Visual programming for the structural assessment of historic masonry structures. *REHABEND* 2020.
- [57] Fortunato A, Fabbrocino F, Angelillo M, Fraternali F. Limit analysis of masonry structures with free discontinuities. *Meccanica* 2018;53(7):1793–802.
- [58] Colombo C, Savalle N, Mehrotra A, Funari MF, Lourenço PB. Experimental, numerical and analytical investigations of masonry corners: Influence of the horizontal pseudo-static load orientation. *Construction and Building Materials* 2022;344. <https://doi.org/10.1016/j.conbuildmat.2022.127969>.
- [59] Casapulla C, Argiento LU, Maione A, Speranza E. Upgraded formulations for the onset of local mechanisms in multi-storey masonry buildings using limit analysis. *Structures* 2021;31:380–94.
- [60] Almeida C, Guedes JP, Arêde A, Costa A. Geometric indices to quantify textures irregularity of stone masonry walls. *Constr Build Mater* 2016;111:199–208.
- [61] Borri A, Corradi M, Castori G, De Maria A. A method for the analysis and classification of historic masonry. *Bull Earthq Eng* 2015;13:2647–65.
- [62] Rhino - Rhinoceros 3D 2020. <https://www.rhino3d.com/> (accessed July 9, 2021).
- [63] Grasshopper - algorithmic modeling for Rhino 2020. <https://www.grasshopper3d.com/> (accessed June 15, 2021).
- [64] Casapulla C, Argiento LU. In-plane frictional resistances in dry block masonry walls and rocking-sliding failure modes revisited and experimentally validated. *Compos Part B Eng* 2018;132:197–213. <https://doi.org/10.1016/J.COMPOSITESB.2017.09.013>.
- [65] The Python Language Reference — Python 3.9.5 documentation 2021. <https://docs.python.org/3/reference/> (accessed June 15, 2021).
- [66] Lagarias JC, Reeds JA, Wright MH, Wright PE. Convergence properties of the Nelder-Mead simplex method in low dimensions. *SIAM J Optim* 1998;9:112–47.
- [67] Cundall PA. A computer model for simulating progressive, large-scale movements in blocky rock systems. *Int Symp Rock Mech*, vol. 2, Nancy; 1971, p. 47–65.
- [68] Lemos JV. Discrete element modeling of the seismic behavior of stone masonry arches. In: G.N. P., Middleton J, Kralj B, editors. *Comput methods Struct Mason*, Florence: E&FN Spon; 1997, p. 220–7.
- [69] Saygılı Ö, Lemos JV. Investigation of the structural dynamic behavior of the frontinus gate. *Appl Sci* 2020;10:5821. <https://doi.org/10.3390/app10175821>.
- [70] Pulatsu B, Erdogmus E, Bretas EM, Lourenço PB. In-Plane Static Response of Dry-Joint Masonry Arch-Pier Structures. *AEI* 2019, Reston, VA: American Society of Civil Engineers; 2019, p. 240–8. <https://doi.org/10.1061/9780784482261.028>.
- [71] Cundall PA, Detournay C. Dynamic relaxation applied to continuum and discontinuum numerical models in geomechanics. *Rock Mech Eng*, CRC Press; 2017, p. 57–102.
- [72] Hart R, Cundall PA, Lemos JV. Formulation of a three-dimensional distinct element model - Part II. Mechanical calculations for motion. *Int J Rock Mech Min Sci Geomech* 1988;25:117–25.
- [73] de Felice G, Fugger R, Gobbin F. Overturning of the façade in single-nave churches under seismic loading. *Bull Earthq Eng* 2021;1–22.
- [74] Casapulla C, et al. Performance-based Seismic Analysis of Rocking Masonry Façades Using Non-linear Kinematics with Frictional Resistances: A Case Study. *International Journal of Architectural Heritage* 2021;15. <https://doi.org/10.1080/15583058.2019.1674944>.
- [75] Valero E, Adán A, Bosché F. Semantic 3D reconstruction of furnished interiors using laser scanning and RFID technology. *J Comput Civ Eng* 2016;30:4015053.
- [76] Valero E, Bosché F, Forster A. Automatic segmentation of 3D point clouds of rubble masonry walls, and its application to building surveying, repair and maintenance. *Autom Constr* 2018;96:29–39.